Energy Equip. Sys./ Vol. 11/No. 1/March 2023/ 29-42

ENERGY EQUIPSYS

Energy Equipment and Systems

http://energyequipsys.ut.ac.ir
www.energyequipsys.com

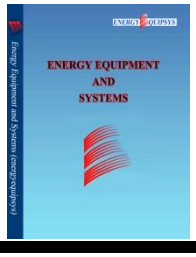

The effect of the linear method on electrochemical impedance spectroscopy calculation in the time domain under the noise condition

Authors

Razieh Hamedi [a*]
Farshad Torabi [a]
Jahan Bakhsh Ghasemi [b]

[a] Mechanical Engineering Faculty, K. N. Toosi University of Technology, Tehran, Iran

[b] Analytical Chemistry Department, Chemistry Faculty, School of Sciences, University of Tehran, Tehran, Iran

Article history:

Received : 20 July 2022
Accepted : 30 September 2022

ABSTRACT

Electrochemical impedance spectroscopy is a powerful tool for determining the behavior of electrochemical systems. Despite being costly and time-consuming, the time-domain impedance calculation of electrochemical systems is advantageous. However, this method exhibits a high error rate under noise conditions. In this study, the linear technique is developed to minimize noise effects when calculating the impedance of electrochemical systems in the time domain. Multiple equivalent circuit samples are simulated, and the linear technique versus the standard fast Fourier transform method for a noisy input is compared. The results indicate that its error rate is considerably less than that of the fast Fourier transform. The error rate in the Li-ion battery equivalent circuit was reduced from 273.5446 using the fast Fourier transform to 0.0049 using the linear method. Notably, this reduction is significant and on the order of 10^5. *Additionally, the decline in the real and imaginary parts of mean relative error is in the order of 10. It is concluded that the linear method results in less error in the presence of noise and is faster than traditional electrochemical impedance spectroscopy in the frequency domain. Thus, the linear method outperforms the fast Fourier transform method in time-domain electrochemical impedance spectroscopy.*

Keywords: Impedance, Electrochemical Systems, Time Domain, Noise, Linear Method

1. Introduction

Electrochemical impedance spectroscopy (EIS) is a suitable technique for identifying the electrochemical systems' behavior. In this method, a system's output voltage or current (depending on the input type) is measured based on a sinusoidal current or voltage input signal with a spectrum of frequencies. Due to the comprehensive investigation of the system, it is necessary to repeat the test above for the entire frequency range, from microhertz to megahertz, as different electrochemical phenomena occur at different frequencies. The frequency response analyzer is then used to determine the system impedance, and the battery parameters are determined based on the system's equivalent circuit. Thus, the stated method necessitates ample time, particularly at low frequencies. In addition, it is necessary to reduce noise to the lowest possible level and apply the correct input signals to maintain the system's steady state. Therefore, expensive devices are needed to employ this method.

Numerous researchers utilized EIS to determine the battery parameters. These

* Corresponding author: Razieh Hamedi
Faculty of Mechanical Engineering K. N. Toosi University of Technology Tehran, Iran
Email: r.hamedi@email.kntu.ac.ir

parameters are adequate for identifying the battery's behavior. Middlemiss et al. [1] studied the internal sodium-ion battery degradation process. Using the EIS, they calculated the battery's impedance and identified its principal degradation mechanisms. In addition, Krikis [2] utilized EIS to determine the degradation performance parameters of the nickel manganese cobalt oxide (NMC) Li-ion batteries. Vyroubal et al. [3] extracted the values of the equivalent circuit parameters, such as resistance and capacitance in the NMC Li-ion battery, from the EIS measurements. Jiang et al. [4] estimated the state of health (SoH) of 18650-type commercial batteries using EIS. The proposed SOH estimation was adaptable to various aging conditions.

Scipioni et al. [5] investigated the 26650 cylindrical commercial LiFePO4/Graphite battery. In this paper, the Li-ion battery was disassembled, and the EIS was used to characterize the two electrodes separately. Ma et al. [6] utilized EIS to investigate the potential effects of the battery's internal short circuit on physical processes at various SOH levels. EIS was employed by Amano et al. [7] to evaluate series resistance and charge-transfer resistance. Under UV-visible light irradiation, they examined the effect of charge transport at the interface between the oxide particles and the conductive substrate using EIS.

EIS was used by Yao et al. [8] to characterize the phenol mass transfer coefficients of composite extractive membranes with varying polydimethylsiloxane thicknesses. They observed a simple correlation between membrane impedance, selective layer thickness, and phenol mass transfer rate. Using the EIS, Jiang et al. [9] determined the relationship between electrochemical impedance and the capacity of aging batteries through EIS. Schmitt et al. [10] used the EIS to investigate the capacity loss and impedance rise of commercial 18650 Lithium-ion batteries due to calendar aging.

Teliz et al. [11] proposed an EIS-based strategy for identifying and measuring the aging mechanisms of commercial 18650 NMC lithium-ion batteries over time. They fitted the EIS spectra to a proper equivalent electrical circuit, and the main mechanisms responsible for the degradation were identified through the calculated parameter variations with time. Koseoglou et al. [12] utilized the EIS to detect Li plating in Li-ion batteries during the charging process. Consequently, lithium plating can be detected by monitoring the real and imaginary components of the battery's impedance in real-time. Ezpeleta et al. [13] used the EIS to characterize commercial cylindrical Li-ion cells under different state of charge (SoC) conditions and up to 300 charge/discharge cycles to determine the SoH status. Captiva et al. [14] investigated the electrochemical reactions occurring in a 3.4 Ah Li-S pouch cell. They characterized the electrode processes, complex interfaces, and internal resistance by utilizing the EIS. Mohsin et al. [15] introduced an innovative method for determining the SoH of the lead-acid battery from the EIS. They proposed a dependable formula to link the SoH and EIS for batteries with an unknown history.

The studies mentioned used EIS to calculate various electrochemical system parameters; however, this method is time-consuming and expensive.

Time-domain measurement is an additional method for determining the behavior of electrochemical systems. This method applies a time-dependent input voltage or current signal to the system. Afterward, the time-dependent current or voltage system response is measured. The impedance can be calculated by dividing the fast Fourier transform (FFT) of the voltage by the FFT of the current. Unlike the EIS, voltage, and current are measured in the time domain, and the frequency domain is calculated using mathematical relations. The primary advantage of the time-domain technique over the EIS is that it reduces the time and cost of the procedure. As stated previously, the EIS method is time-consuming.

Lohman et al. [16] evidenced that the EIS method requires more time than electrochemical impedance spectroscopy in the time domain. They employed time domain analysis to generate impedance spectra for the SoC estimate of Li-ion batteries, considering the effects of aging. In addition to sinusoidal waveforms, they used rectangular, Gaussian, and $\sin(x)/x$ pulses for EIS in a time domain and reduced the measurement time for EIS. In addition, Klotz [17] compared the EIS method to electrochemical impedance spectroscopy in

the time domain and concluded that the required time for impedance spectroscopy in the frequency domain is nearly three times that of the time-domain measurement. Numerous researchers employed the electrochemical impedance spectroscopy technique in the time domain to address this issue.

Hallemans et al. [18] characterized commercial LG M50 batteries using EIS in the time domain. This study provided a novel time-domain EIS (operando EIS) for evaluating time-varying impedance data of Li-ion batteries. Kuipers et al. [19] utilized EIS in the time domain to develop an efficient method designed to operate on a battery management system continuously measuring electrochemical impedance by analyzing battery current and voltage readings iteratively. Furthermore, the algorithm adapted the parameters of an equivalent circuit model to best match the battery's impedance, providing characteristic measures of a battery's internal conditions.

Islam et al. [20] introduced an online EIS method for a Li-Ion battery. They employed EIS in the time domain to precisely measure impedance using this technique. The proposed spectroscopic method was beneficial for monitoring and evaluating the electrochemical conditions of a battery. Messing et al. [21] used EIS in the time domain to capture the SoH of the battery relaxation effect. They proposed an SoH estimation method that combined fractional order impedance modeling and short-term relaxation effects with EIS characterization for rapid SoH determination.

Tairov et al. [22] proposed an estimation technique for the valve-regulated lead-acid battery SOC using electrochemical impedance spectroscopy in the time domain. De Angelis et al. [23] characterized the 18650 Li-ion battery using EIS in the time domain. They utilized the multisine function as an input excitation signal in the time domain and studied the battery's impedance Nyquist plot. Fu et al. [24] estimated the SoH of the Li-ion battery using the EIS in the time domain. From the perspective of the EIS in the time domain, they proposed a fast impedance-based battery SOH estimation method for Li-ion batteries based on impedance calculation.

Previous studies stated above used the EIS in the time domain to reduce the time required for the characterization of electrochemical systems, but they employed filters to reduce the impact of noise on the calculation of impedance using the conventional FFT.

Noise prevents the estimation of a suitable equivalent circuit using the EIS method. In addition, if semicircles overlap in certain areas of the Nyquist plot, noise makes initial estimation more difficult. Therefore, noise is one of the difficulties of electrochemical impedance spectroscopy in the time domain [25]. Theoretically and in the absence of noise, it is possible to obtain appropriate responses using the FFT method, but using the FFT method in the presence of noise results in error. One way to reduce error in the presence of noise is to increase the integration order of the Fourier transform (FT). Klotz [26] was the first to propose using a linear method to increase the order of FT integration. In this reference, however, the effectiveness of noise in the response of various circuits prior to and following the linear method is not discussed in detail. In addition, the acceptable range of varying circuit parameter values required to achieve the desired response is not investigated.

This paper examines the significance of the linear method for calculating impedance from time-domain measurements. In order to demonstrate its effect on the noise calculation, series and parallel circuits and equivalent circuits of the battery are simulated in the presence of noise, and the correct range of parameters for the series and parallel circuits is determined to achieve the desired response. In all simulations, the FFT and linear integration are used, demonstrating that linear integration is superior to the FFT method. The novelty and major contributions of the present study can be summarized as: (a) Development of the linear method in calculating electrochemical impedance spectroscopy, (b) Real-time simulation of electrochemical systems in the presence of noise, (c) Calculating the electrochemical system impedance using the linear and conventional FFT methods and comparing the resulting errors from these two methods (d) Determining the suitable range of the electrochemical system's parameters in the linear method to achieve proper impedance values of the electrochemical systems. The remaining sections of the paper are organized

as follows. The discussion is covered in Section 2, while the methodology of the proposed method is presented in Section 3. Section 4 presents the results, and Section 5 provides concluding remarks.

Nomenclature

a_V	constant coefficient of the estimated straight line of voltage between the t_n and t_{n+1} time points	
b_V	constant coefficient of an estimated straight line of voltage between the t_n and t_{n+1} time points	F
C	capacitance	
C_n	the double-layer capacitance of the negative electrode	F
C_p	the double-layer capacitance of the positive electrode	F
F_k	discrete Fourier transform of the function f at k frequency	
f_i	value of the function f at the i_{th} point	
f(t)	arbitrary function	
FFT	fast Fourier transform	
FT	Fourier transform	
f(ω)	Fourier transform of arbitrary function f (t)	
I	current,	A
I(ω)	Fourier transform of the current	
$Im_I(\omega)$	the imaginary part of the current Fourier transform	
$Im_V(\omega)$	imaginary part of the voltage Fourier transform	
i	counter of the number of points	
n	beginning of integration interval	
N	measured data number	
R	resistance	Ω
R_1	resistance	Ω
R_2	resistance	Ω
R_e	electrolyte resistance	Ω
R_n	resistance of a negative electrode	Ω
R_p	resistance of a positive electrode	
$Re_I(\omega)$	the real part of current Fourier transform	Ω
$Re_V(\omega)$	real part of voltage Fourier transform	
SoC	state of charge	
SoH	state of health	
t	time,	s
V	voltage,	v
V_s	voltage source,	v
V (ω)	Fourier transform of voltage	
w_i	the inverse of the square of the vector length of impedance in the i_{th} frequency	
Z(ω)	impedance	Ω
$Z_{a,i}$	analytical impedance in the i_{th} frequency	Ω
$Z_{im,i}$	the measured imaginary part of impedance in the i_{th} frequency	Ω
$Z_{ima,i}$	the analytical imaginary part of impedance in the i_{th} frequency	Ω
Z_p	parallel circuit impedance	Ω
Z_r	Randles circuit impedance	Ω
$Z_{re,i}$	measured real part of impedance in the i_{th} frequency	Ω
$Z_{rea,i}$	the analytical real part of impedance in the i_{th} frequency	Ω
Z_s	series circuit impedance	Ω
Greek		
Δ_{im}	mean relative error of imaginary part of impedance	
Δ_{re}	mean relative error of the real part of the impedance	
ω	frequency	Hrtz

2. Discussion

The FT of each $f(t)$ function is defined as $f(\omega)$, calculated based on Eq. (1):

$$f(\omega)=\int_{-\infty}^{\infty} f(t)\exp(-j\omega t)dt \quad (1)$$

where ω and t represent frequency and time, respectively. Since input/output data are discrete in time-domain measurements of electrochemical systems, FFT is typically used to convert functions from the time domain to the frequency domain.

Moreover, FFT is applied to discrete points according to Eq. (2).

$$F_k=\sum_{i=0}^{N-1} f_i \exp\left(-j\left(\frac{2\pi i}{N}\right)k\right) \quad k=0..N-1 \quad (2)$$

In this equation, F_k represents the FT of the function f at frequency k. Furthermore, N indicates the number of points, i denotes the index of the number of points, and f_i is the value of the function f at the i_{th} point.

In the absence of noise, the FFT method is ideally suited for obtaining impedance due to its high accuracy (the closeness of the impedance obtained by numerical FT to the impedance obtained by the analytical method). However, when noise is present, this method's error rate increases. Due to the necessity of dividing the FT of voltage by the FT of current when calculating the impedance of electrochemical systems, the

error of the impedance calculation increases, making it impossible to calculate the impedance accurately. Assume, for example, that the FT of the voltage and current are computed using the FFT method with an accuracy of 10^{-6} and 10^{-8}, respectively. Therefore, the voltage and current have been calculated with reasonable accuracy. However, to calculate the impedance, the voltage FT is divided by the current FT, resulting in an error of the order of 100, which is unacceptable. Therefore, the FFT method is unsuitable for calculating impedance in the presence of noise, and it is preferable to use a higher-order method to calculate the numeric FT in noisy conditions accurately.

This paper explores the effect of the linear method and electrochemical systems' parameters on the time domain impedance calculation of electrochemical systems in the presence of noise.

3. Methodology

According to Eq. (1), the FT of the voltage $V(t)$ and current $I(t)$ can be obtained by the following equations:

$$V(\omega)=\int_{-\infty}^{+\infty}V(t)\exp(-j\omega t)dt \tag{3}$$

$$I(\omega)=\int_{-\infty}^{+\infty}I(t)\exp(-j\omega t)dt \tag{4}$$

On the other hand, Euler's formula is expressed via the following equation:

$$\exp(-j\omega t)=\cos(\omega t)-j\sin(\omega t) \tag{5}$$

By substituting Eq.(5) in (3) and assuming positive time values, Eq. (6) is obtained as follows:

$$V(\omega)=\int_{0}^{+\infty}V(t)\cos(\omega t)dt-j\int_{0}^{+\infty}V(t)\sin(\omega t)dt \tag{6}$$

As can be seen, Eq. (6) consists of a real and an imaginary part, defined as follows:

$$Re_V(\omega)=\int_{0}^{+\infty}V(t)\cos(\omega t)dt \tag{7}$$

$$Im_V(\omega)=-\int_{0}^{+\infty}V(t)\sin(\omega t)dt \tag{8}$$

Equation (9) is therefore obtained by substituting Eqs. (7) and (8) in Eq.(6):

$$V(\omega)=Re_V(\omega)+jIm_V(\omega) \tag{9}$$

Similarly, the current is obtained according to Eq. (10).

$$I(\omega)=Re_I(\omega)+jIm_I(\omega) \tag{10}$$

Therefore, integration is required to obtain the FT of any function. Numerous numerical integration methods are available, including the midpoint, trapezoidal rule, Simpson, and others. As depicted in Fig. 1(a), the FFT method employs a constant degree method, which is quite similar to the midpoint rule. The linear method and the trapezoidal integration method are identical. Figure 1(a) illustrates the FFT method, whereas Fig. 1(b) depicts the linear method. Figure 1(a) shows the one-point method for calculating the Fourier transform, which means that at a given frequency, only one-point data is used to calculate the Fourier transform. Nevertheless, Fig. 1(b) displays the two-point or linear method for calculating the Fourier transform, indicating that two-point data is used to calculate the Fourier transform at a given frequency. Consequently, two points are used to draw a straight line, which is then utilized to calculate the Fourier transform. Equations (7) and (8) are transformed as shown in Fig. 1(b) to perform a linear integration:

$$Re_V(\omega)=\sum_{n=1}^{N-1}\int_{t_n}^{t_{n+1}}(a_V t+b_V)\cos(\omega t)dt \tag{11}$$

$$Im_V(\omega)=-\sum_{n=1}^{N-1}\int_{t_n}^{t_{n+1}}(a_V t+b_V)\sin(\omega t)dt \tag{12}$$

$$Re_V(\omega)=\sum_{n=1}^{N-1}\left[\left(\frac{a_V t+b_V}{\omega}\right)\sin(\omega t)+\frac{a_V}{\omega^2}\cos(\omega t)\right]_{n}^{n+1} \tag{13}$$

$$Im_V(\omega)=\sum_{n=1}^{N-1}\left[\left(\frac{-a_V t-b_V}{\omega}\right)\cos(\omega t)+\frac{a_V}{\omega^2}\sin(\omega t)\right]_{n}^{n+1} \tag{14}$$

where a_V and b_V denote the constant coefficients of the linear voltage between the t_n and t_{n+1} time points. Also, t_n and t_{n+1} are the beginning and end of the integration interval. Moreover, N represents the measured data number, and for each two subsequent data points of t_n and t_{n+1}, the corresponding voltages are V_n and V_{n+1}, respectively. According to Fig. 1(b), V_n and V_{n+1} can be obtained using Eqs. (15) and (16).

$$V_n=a_V t_n+b_V \tag{15}$$

$$V_{n+1}=a_V t_{n+1}+b_V \tag{16}$$

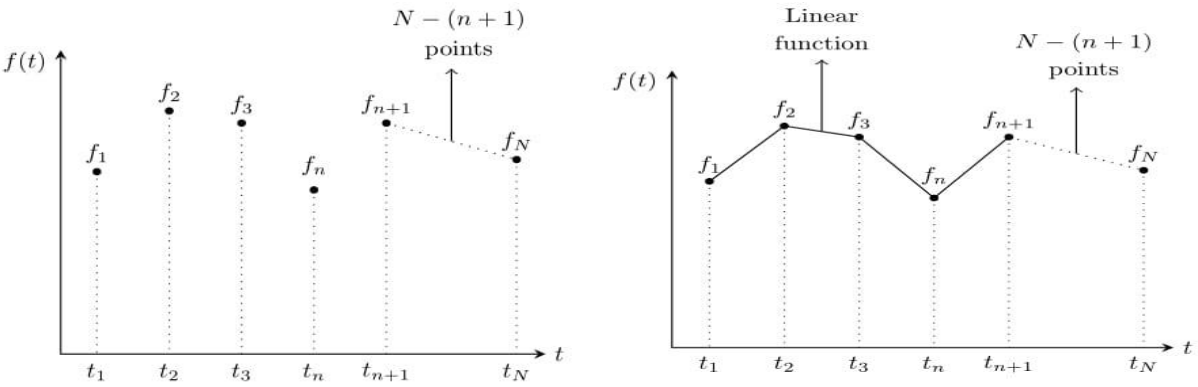

(a) Description of the FFT method (b) Description of the linear FT

Fig. 1. Description of the FFT and linear FT

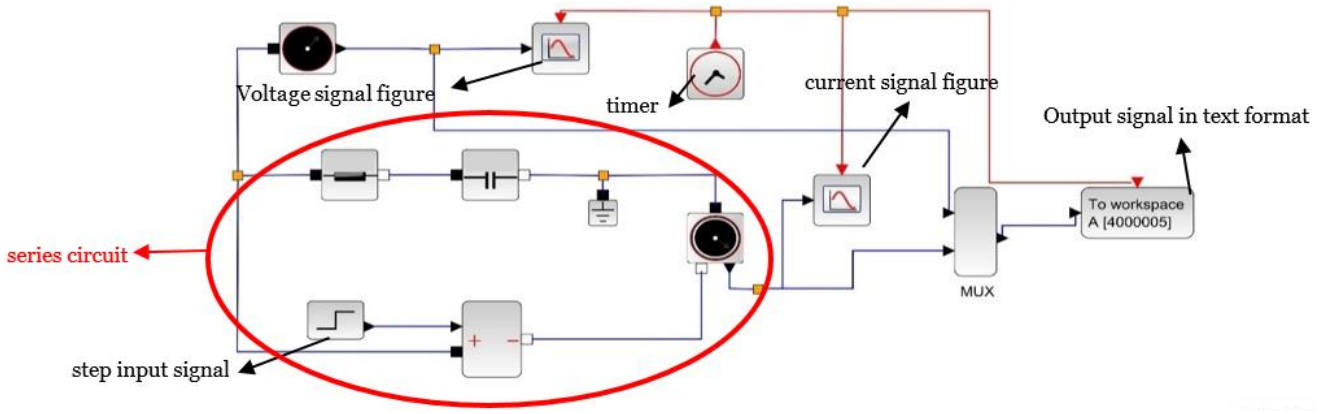

(a) The series circuit in Scilab software

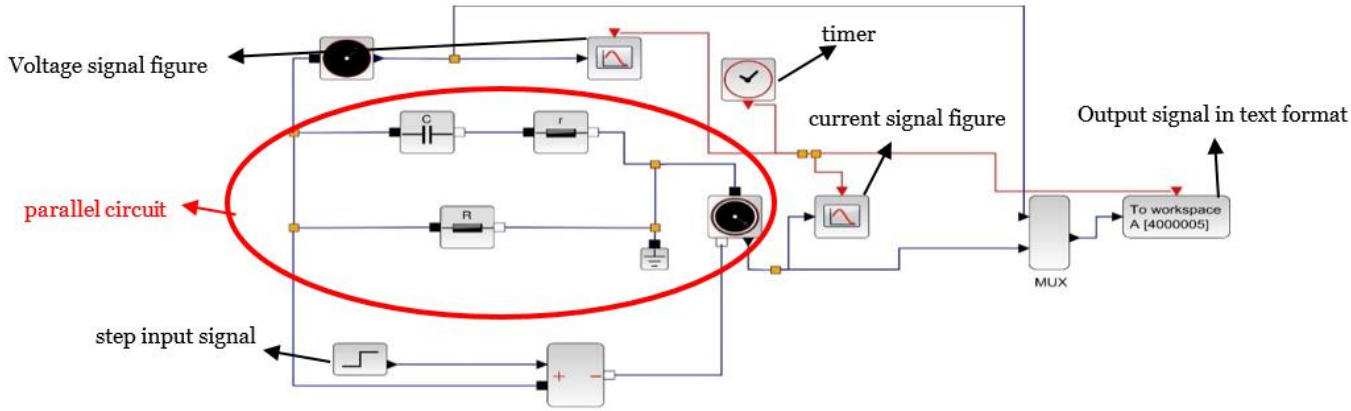

(b) The parallel circuit in Scilab software

Fig. 2. The series and parallel circuits in Scilab software

The same method applies to calculating the FT of the current. The impedance is the ratio of the FT of the voltage to the FT of the current; therefore, $Z(\omega)$ can be calculated using the following equation:

$$Z(\omega)=\frac{V(\omega)}{I(\omega)} \tag{17}$$

The linear method is validated in this paper by applying the present procedure to two classical circuits. Circuit one contains a capacitor (C) and a resistor (R) in series in Scilab software, shown in Fig. 2(a). Circuit two exhibits the same elements in parallel in Scilab software, as depicted in Fig. 2(b). Finally, to verify a more realistic circuit for the battery simulation, the same method is then applied to the Randles circuit, which is widely used to predict the behavior of lithium batteries. Scilab is a free, cross-platform, open-source numerical computing package and a high-level, numerically-oriented programming language. It is applicable for signal processing. In this software, every circuit parameter, such as a resistor, capacitor, and voltage source, is arranged, and the output signal can be recorded and analyzed for any input signal.

3.1. Series and parallel circuits

The impedance of the series and parallel circuits can be calculated according to Eqs. (18) and (19):

$$Z_s=R+\frac{1}{jC\omega} \tag{18}$$

$$Z_p=\frac{R}{1+jRC\omega} \tag{19}$$

In these equations, Z_s, Z_p, and ω represent series circuit impedance, parallel circuit impedance, and frequency, respectively. Also, R and C denote capacitor capacity and ohmic resistance. Furthermore, the impedance Nyquist plot of the series and parallel circuits according to Eqs. (18) and (19) are shown in Figs. 3(a) and 3(b), respectively.

3. 2. Battery model

The Randles model is among the simplest and most prominent models in electrochemical systems, such as batteries. According to Fig. 4(a), for each electrode in the model above, a circuit consisting of a parallel resistor and capacitor in series with a resistor is considered. *R1* and *R2* represent the resistors, and *C* represents the capacitor. To this end, since batteries consist of two electrodes, each electrode comprises a Randles circuit configured per Fig. 4(b), where R_n, R_p, C_n, C_p, and R_e denote the resistance of the negative electrode, the resistance of the positive electrode, the capacitance of the negative electrode, the capacitance of the positive electrode, and the electrolyte resistance, respectively. Numerous studies have examined this Li-ion battery model.

Nicolian et al. [27] used this model to characterize three types of Li-ion batteries (NMC, LFP, and LTO). This model was developed by Madani et al. [28] for the LTO Li-ion battery. The circuit impedance shown in Fig. 4(b) is calculated theoretically based on:

$$Z_r=\frac{R_n}{1+jR_nC_n\omega}+\frac{R_p}{1+jR_pC_p\omega}+R_e \tag{20}$$

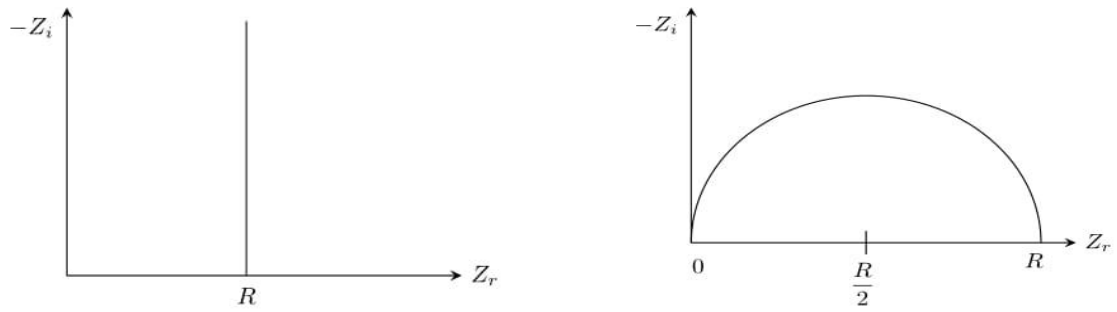

(a) The series circuit (b) The parallel circuit

Fig. 3. The impedance Nyquist plot of the series and parallel circuits

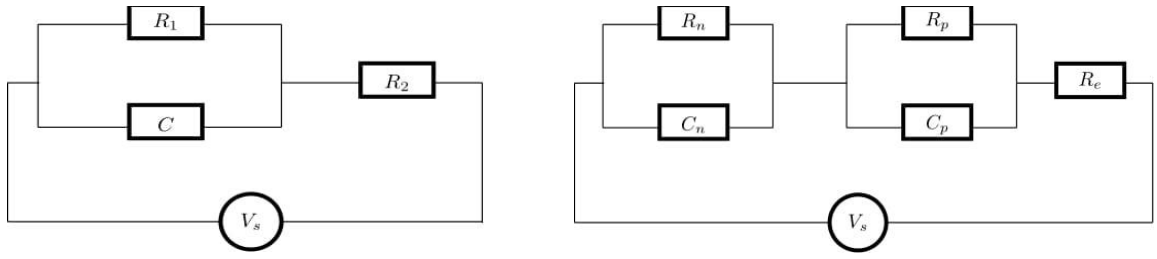

(a) Randles model (b) Equivalent circuit of a Lithium-ion battery sample

Fig. 4. Electrode and battery model

In the present paper, numerous simulations with different values for R and C were performed. Numerous conditions (hundreds of cases) were simulated in the software Scilab; however, not all simulations are included in this article. In order to demonstrate the linear method, one of the simulation conditions listed in Table 1 is applied to the series, parallel, and battery circuits. According to Fig. 5, the input signal in these simulations is a noisy step pulse in 150 seconds with a height of 4.2 volts.

4. Results

4. 1. Series and parallel circuits

Figures 6(a) and 6(b) depict the impedance Nyquist plot in the condition specified in Table 1 for the series circuit using the FFT and linear method, respectively. According to Fig. 3(a), the impedance Nyquist plot is a vertical line intersecting the horizontal axis at 1000 Ω. According to Figs. 6(a) and 6(b), the vertical line is not obtained precisely due to the presence of noise, and the error is present in both methods.

This paper calculates the error using the complex nonlinear least square (CNLS) method. The CNLS method is a technique for approximating a model with a linear one and refining the model's parameters through successive iterations. This method identifies the appropriate model by minimizing Eq. (21), representing the object function [29].

$$s=\sum_{i=1}^{N}\omega\left(\left(Z_{re,i}-Z_{rea,i}\right)^2+\left(Z_{im,i}-Z_{ima,i}\right)^2\right) \qquad (21)$$

In this equation, w_i denotes the inverse square of impedance magnitude. Moreover, $Z_{re,i}$ and $Z_{rea,i}$ represent the real part of the measured and analytical impedance at the i_{th} frequency, respectively. Additionally, $Z_{im,i}$ and $Z_{ima,i}$ denote the imaginary part of measured and analytical impedance at the i_{th} frequency, respectively. This equation has been considered in this paper to determine the error rate of the impedance diagram. This equation's lower values indicate the corresponding technique's lower error, with zero representing the lowest possible value. Consequently, the error rate decreases, as this value approaches zero.

A second CNLS method suitability criterion for the fitted impedance diagram [29] is represented by

$$\Delta_{re}=\sum_{i=1}^{N}\frac{Z_{re,i}-Z_{rea,i}}{|Z_{a,i}|}, \qquad (22)$$

$$\Delta_{im}=\sum_{i=1}^{N}\frac{Z_{im,i}-Z_{ima,i}}{|Z_{a,i}|} \qquad (23)$$

In these equations, Δ_{re} and Δ_{im} specify the residual value of the real and imaginary parts of the impedance at the i_{th} frequency, respectively. Also, $Z_{a,i}$ is the analytical impedance in the i_{th} frequency.

Equations (22) and (23) vary in value at various frequencies. In this study, the average of these equations has been used to calculate the relative error. The mean of Eqs. (22) and (23) has, respectively, been calculated using

$$\Delta_{re}=\frac{1}{N}\sum_{i=1}^{N}\left|\frac{Z_{re,i}-Z_{rea,i}}{|Z_{a,i}|}\right| \qquad (24)$$

$$\Delta_{im}=\frac{1}{N}\sum_{i=1}^{N}\left|\frac{Z_{im,i}-Z_{ima,i}}{|Z_{a,i}|}\right| \qquad (25)$$

In these equations, N represents the quantity of measured data. Similar to the previous paragraph, as the value of these equations decreases, the error rate decreases, and the appropriateness of the corresponding method increases.

Using Eqs. (21) to (25), the values of Δ_{re}, Δ_{im}, and s, through the FFT and linear methods in a series circuit, are shown in Table 2. According to this table, the Δ_{re}, Δ_{im}, and s of the FFT method are greater than the linear method. Therefore, in the linear method, the impedance Nyquist has a smaller amount of error compared to the analytical method.

The same elements from table 1 are used in the parallel circuit, and the FFT and linear methods results are shown in Figs. 7(a) and 7(b),

Table 1. Conditions of the sample test

$R(\Omega)$	C(F)	Time(s)	Time step(s)	Vs (v)
1000	0.001	150	0.001	Noisy step pulse (Fig. 5)

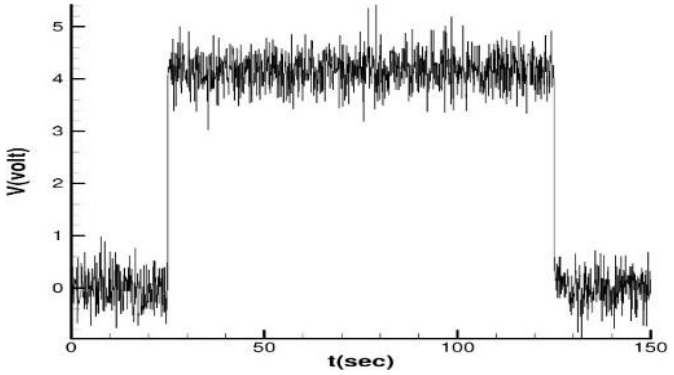

Fig. 5. The noisy step pulse as the input signal

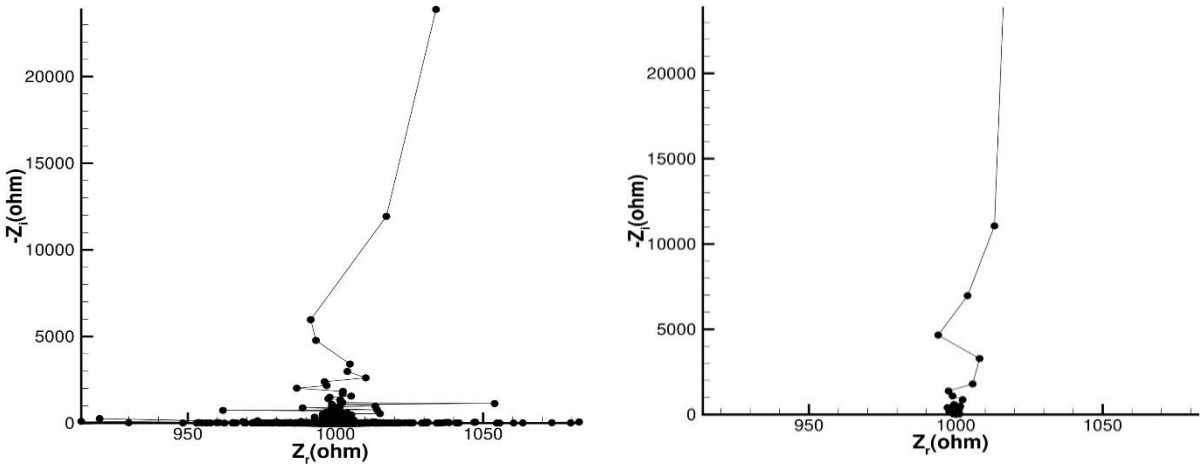

(a) FFT method **(b) Linear method**

Fig. 6. Impedance Nyquist plot of the series circuit following Table 1's conditions. Utilizing FFT and the linear method

Table 2. The errors in the series circuit

	FFT	Linear
Δre	8.3910×10^{-4}	8.2509×10^{-4}
Δim	0.0025	7.9347×10^{-4}
s	38.3623	8.9303×10^{-5}

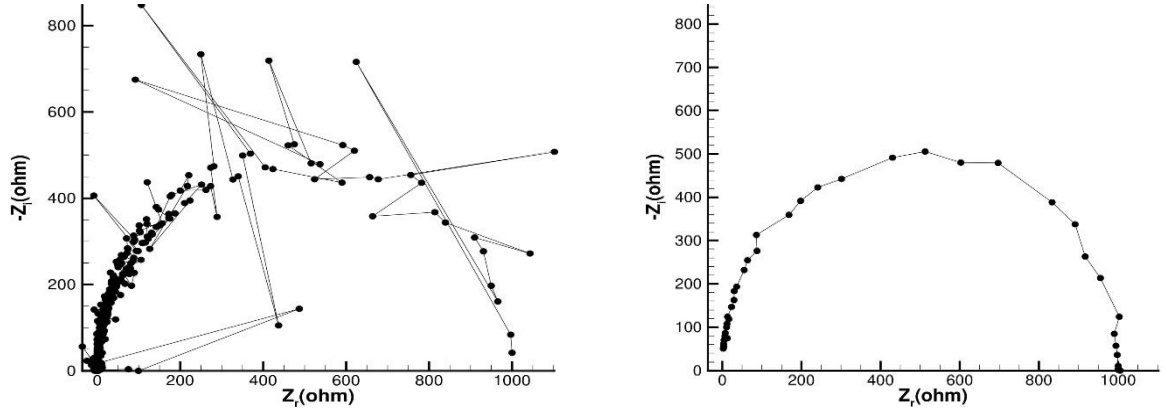

(a) FFT method (b) Linear method

Fig. 7. Impedance Nyquist plot of the parallel circuit in the condition as per Table 1 using the FFT and linear method

Table 3. The errors in the parallel circuit

	FFT	Linear
Δre	1.6033	0.0116
Δim	7.9358	0.0087
s	2.9327×10^{7}	0.0242

respectively. As can be seen, the linear method yields the impedance Nyquist plot as a semicircle that intersects the horizontal axis at 1000 Ω. It follows the analytical method (Fig. 3(b)). However, as shown in Fig. 7(a), the FFT method has a high error.

The value of Δ_{re}, Δ_{im}, and s in a parallel circuit using the FFT and linear method is shown in Table 3. According to this table, the Δ_{re}, Δ_{im}, and s of the FFT method are greater than the linear method. As a result, the linear method exhibits less distinction than the analytical method in both series and parallel circuits; thus, it is an appropriate method for calculating numerical FT and, consequently, the impedance of electrochemical systems.

4. 2. Determination of the acceptable values for R and C

More than a thousand simulations were performed with different R and C values to study the effect of various circuit parameters. Notably, the numerical errors were strongly dependent on the values of R and C. Consequently, it would be necessary to determine the acceptable error ranges for these values. Figure 8(a) depicts the Nyquist plot of the sample simulation in the series circuit based on Table 1 and changing the resistance value to 0.001 Ω using the linear method. As stated, a vertical line is not displayed by selecting the circuit parameters in the high error range (Table 4). Figure 8(b) depicts the Nyquist diagram with the capacitance value changed to 0.01 F, which is in the low error range (according to Table 4). In contrast to the previous simulation with a capacitance of 0.001 F, the Nyquist plot is nearly vertical and intersects the horizontal axis at the value of the ohmic resistor. According to Table 4, a high error rate will be present in the responses if $RC > 4$ or $RC < 10^{-5}$. The RC represents the circuit's time constant. According to the simulations, its value must fall within the acceptable error range shown in table 4 to produce the desired results.

Figure 9(a) depicts the Nyquist diagram of another simulation in the parallel circuit, according to Table 1, with the resistance value changed to 0.01 Ω. As can be seen in Table 5, the parallel circuit parameters are selected within the high error range; consequently, no correct answer can be derived from these parameter values. In addition, the FFT method has a high error rate within the specified range of the method presented in this paper; therefore, this method does not produce an accurate answer. Figure 9(b) depicts the Nyquist diagram

of another simulation in the parallel circuit with a resistance value compared to the previous simulation, and the capacitance value changed to 0.1 F. According to Table 5, the semicircle Nyquist plot can be attained if the parallel circuit parameters are selected within the low error range. According to Table 5, if $RC \leq 10^{-5}$, the acquired responses will contain a substantial amount of error. As stated previously, the RC component represents the circuit's time constant. Simulations indicate that appropriate responses will be obtained if this parameter's value falls within the acceptable error range shown in Table 5.

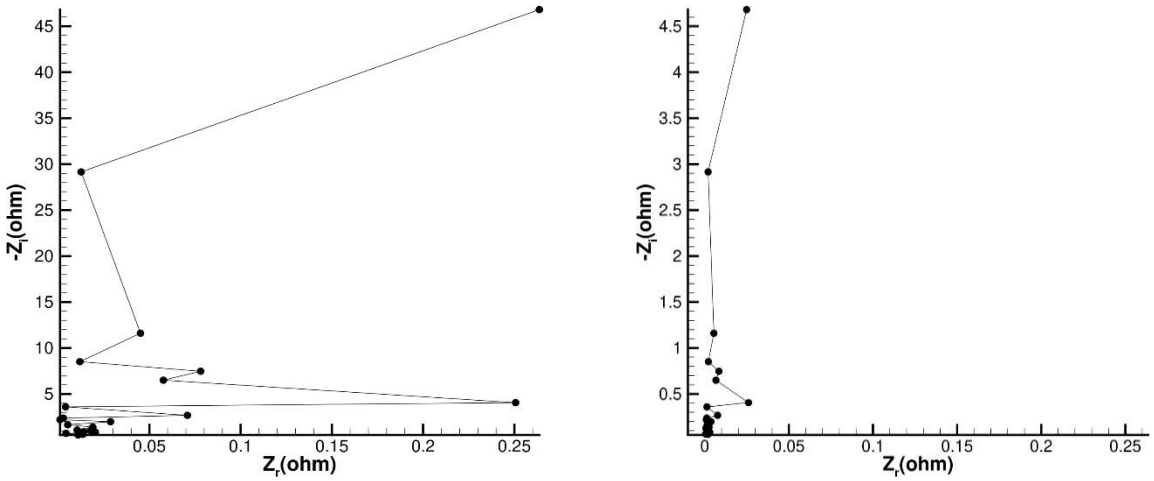

(a) high error range (R=0.001 Ω, C=0.001 F) (b) low error range (R=0.001 Ω, C=0.01 F)

Fig. 8: Impedance Nyquist plot of the series circuit in low and high error range using the linear method

Table 4. The effect of capacitor and resistor values on the impedance of series circuits arrangement in the presence of noise

C (F)	Acceptable error, R (Ω)	High-error, R (Ω)	Acceptable error, RC (ΩF)	High-error, RC (ΩF)
0.001	$10^{-2} \leq R \leq 4000$	$R < 10^{-2}$, $R > 4000$	$10^{-5} \leq RC \leq 4$	$RC > 4$, $RC < 10^{-5}$
0.01	$10^{-3} \leq R \leq 400$	$R < 10^{-3}$, $R > 400$	$10^{-5} \leq RC \leq 4$	$RC > 4$, $RC < 10^{-5}$
0.1	$10^{-4} \leq R \leq 40$	$R < 10^{-4}$, $R > 40$	$10^{-5} \leq RC \leq 4$	$RC > 4$, $RC < 10^{-5}$
1	$10^{-5} \leq R \leq 4$	$R < 10^{-5}$, $R > 4$	$10^{-5} \leq RC \leq 4$	$RC > 4$, $RC < 10^{-5}$
10	$10^{-6} \leq R \leq 0.4$	$R < 10^{-6}$, $R > 0.4$	$10^{-5} \leq RC \leq 4$	$RC > 4$, $RC < 10^{-5}$

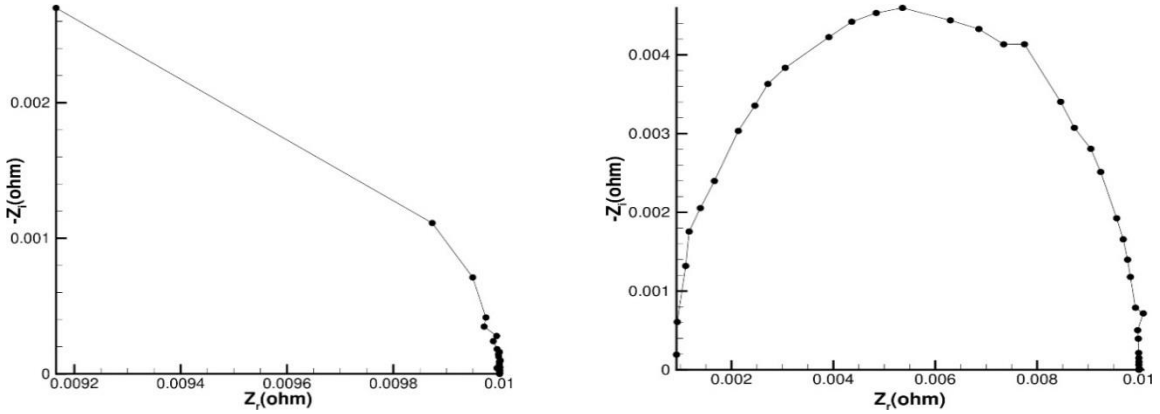

(a) high error range (R=0.001 Ω, C=0.001 F) (b) low error range (R=0.001 Ω, C=0.1 F)

Fig. 9. Impedance Nyquist plot of the parallel circuit in low and high error range using the linear method

Table 5. The effect of capacitor and resistor values in the circuit impedance of parallel configuration in the presence of noise

C (F)	Acceptable error, R (Ω)	High-error, R (Ω)	Acceptable error, RC (ΩF)	High-error, RC (ΩF)
0.001	$R > 10^{-2}$	$R \leq 10^{-2}$	$RC > 10^{-5}$	$RC \leq 10^{-5}$
0.01	$R > 10^{-3}$	$R \leq 10^{-3}$	$RC > 10^{-5}$	$RC \leq 10^{-5}$
0.1	$R > 10^{-4}$	$R \leq 10^{-4}$	$RC > 10^{-5}$	$RC \leq 10^{-5}$
1	$R > 10^{-5}$	$R \leq 10^{-5}$	$RC > 10^{-5}$	$RC \leq 10^{-5}$
10	$R > 10^{-6}$	$R \leq 10^{-6}$	$RC > 10^{-5}$	$RC \leq 10^{-5}$

4. 3. Battery model

To validate the linear method presented in this paper, it is applied to a real NMC Lithium-ion battery ($LiNi_{0.33}Mn_{0.33}Co_{0.33}O_2$). A Randles model with parameters specified in Table 6 has been selected for this battery. In the presence of noise, the analytical equivalent circuit of the battery is compared between the FFT and linear methods. Figures 10(a) and (b) are the results of the FFT and linear methods, respectively. The analytical solution is identical to Eq. (20). Table 7 displays the values of Δ_{re}, Δ_{im}, and s derived from the FFT and linear method.

According to the table, the FFT method exhibits a greater Δ_{re}, Δ_{im}, and s than the linear method. On the other hand, the FFT produces a significant amount of error. In addition, the number of data obtained with the FFT method is greater than with the linear method. In determining the behavior of the battery in the presence of noise, the linear method is, therefore, superior to the FFT method.

Table 6. The actual value of the NMC Lithium-ion battery parameters [3]

SoC	Voc (v)	R_e(Ω)	R_n (Ω)	C_n (F)	R_p (Ω)	C_p (F)
1	4.195754	0.01889	0.001540	1.241	0.002314	4.626

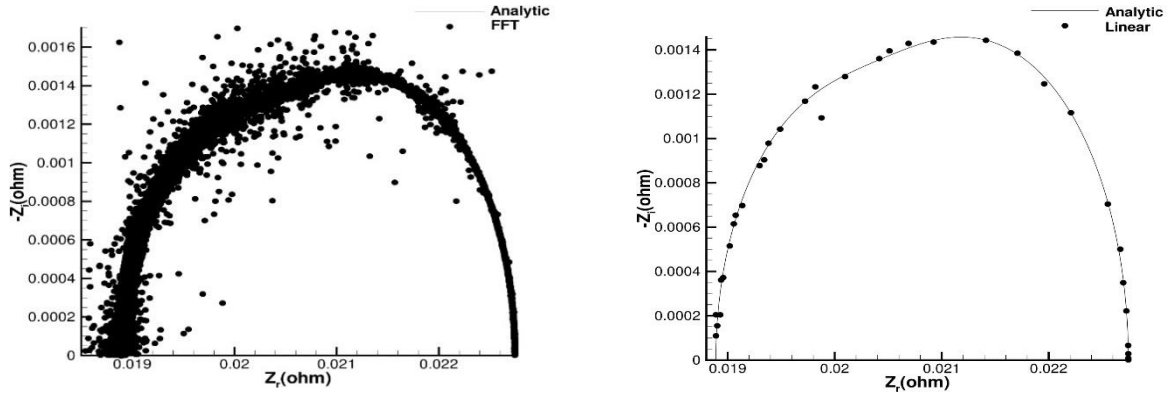

(a) Comparison of the FFT and analytic method

(b) Comparison of the linear and analytic method

Fig.10. Impedance Nyquist plot of battery equivalent circuit using the FFT and linear method at SoC = 1 for the noisy step pulse as the input signal (Fig. 4) in 150 seconds duration with a time step of 0.001 second

Table 7. The errors in the battery model

	FFT	Linear
Δ_{re}	0.0122	0.0019
Δ_{im}	0.0246	0.0062
s	273.5446	0.0049

5. Conclusions

This study developed the linear numerical technique for calculating the impedance of electrochemical systems in the time domain under noise conditions. In this paper, series, parallel, and battery circuits are simulated in the presence of noise using the Scilab software, and their impedance is calculated using the FFT and linear method in the time domain measurement. Then, the appropriate parameter ranges for the circuits are investigated. The linear method has been found to correspond well with analytical data. In the presence of noise, its relative error is significantly lower than conventional FFT. Another result demonstrates that if the conditions $RC > 4$ and $RC < 10^{-5}$ are met for all capacitor values in a series circuit, a significant amount of error will occur in the responses, and if the condition $RC \leq 10^{-5}$ is met for all capacitor values in a parallel circuit, a considerable amount of error will occur in the responses.

Finally, the battery model for the NMC lithium-ion battery with actual parameter values was compared with the analytical method to validate the linear method. In addition, the impedance of the battery model was calculated using the FFT method. It was observed that the linear method is more compatible with the analytical method and produces fewer errors than the FFT method. Consequently, this method is suitable for calculating the impedance of electrochemical systems, including batteries.

References

[1] L. A. Middlemiss, A. J. Rennie, R. Sayers, and A. R. West, "Characterization of batteries by electrochemical impedance spectroscopy," Energy Reports, vol. 6, pp. 232–241, 2020.

[2] G. Krikis, "Diagnostic of lithium-ion batteries," Master's thesis, Aalborg University, Denmark, 2018.

[3] P. Vyroubal and T. Kazda, "Equivalent circuit model parameters ex- traction for lithium-ion batteries using electrochemical impedance spectroscopy," Journal of Energy Storage, vol. 15, pp. 23–31, 2018.

[4] B. Jiang, J. Zhu, X. Wang, X. Wei, W. Shang, and H. Dai, "A comparative study of different features extracted from electrochemical impedance spectroscopy in state of health estimation for lithium-ion batteries," Applied Energy, vol. 322, p. 119502, 2022.

[5] R. Scipioni, P. S. Jørgensen, C. Graves, J. Hjelm, and S. H. Jensen, "A physically-based equivalent circuit model for the impedance of a lifepo4/graphite 26650 cylindrical cell," Journal of The Electrochemical Society, vol. 164, no. 9, p. A2017, 2017.

[6] R. Ma, J. He, and Y. Deng, "Investigation and comparison of the electrochemical impedance spectroscopy and internal resistance indicators for early-stage internal short circuit detection through battery aging," Journal of Energy Storage, vol. 54, p. 105346, 2022.

[7] F. Amano and S. Koga, "Electrochemical impedance spectroscopy of wo3 photoanodes on different conductive substrates: the interfacial charge transport between semiconductor particles and ti surface," Journal of Electroanalytical Chemistry, p. 116685, 2022.

[8] L. Yao, Q. Cheng, Z. Long, Z. Chen, Z. Lin, Y. Li, Y. Tian, and Y. Liao, "Characterizing phenol mass transfer coefficients of composite extractive membranes with different pdms thicknesses by electrochemical impedance spectroscopy," Journal of Water Process Engineering, vol. 49, p. 103057, 2022.

[9] J. Jiang, Z. Lin, Q. Ju, Z. Ma, C. Zheng, and Z. Wang, "Electrochemical impedance spectra for lithium-ion battery aging considering the rate of discharge ability," Energy Procedia, vol. 105, pp. 844–849, 2017.

[10] J. Schmitt, A. Maheshwari, M. Heck, S. Lux, and M. Vetter, "Impedance change and capacity fade of lithium nickel manganese cobalt oxide-based batteries during calendar aging," Journal of Power Sources, vol. 353, pp. 183–194, 2017.

[11] E. Teliz, C. F. Zinola, and V. D´ıaz, "Identification and quantification of aging mechanisms in li-ion batteries by electrochemical impedance spectroscopy." Electrochimica Acta, vol. 426, p. 140801, 2022.

[12]M.Koseoglou, E. Tsioumas, D. Ferentinou,

N. Jabbour, D. Papagian- nis, and C. Mademlis, “Lithium plating detection using dynamic electrochemical impedance spectroscopy in lithium-ion batteries,” Journal of Power Sources, vol. 512, p. 230508, 2021.

[13] I.Ezpeleta, L.Freire, C. Mateo-Mateo, X. R. No´voa, A. Pintos, and S.Valverde-P´erez, “Characterization of commercial li-ion batteries using electrochemical impedance spectroscopy,” ChemistrySelect, vol. 7, no. 10, p. e202104464, 2022.

[14] D. Capkova, V. Knap, A. S. Fedorkova, and D.-I. Stroe, “Analysis of 3.4 ah lithium-sulfur pouch cells by electrochemical impedance spectroscopy,” Journal of Energy Chemistry, 2022.

[15] M. Mohsin, A. Picot, and P. Maussion, “A new lead-acid battery state- of-health evaluation method using electrochemical impedance spectroscopy for second life in rural electrification systems,” Journal of Energy Storage, vol. 52, p. 104647, 2022.

[16] N. Lohmann, P. Weßkamp, P. Haußmann, J. Melbert, and T. Musch, “Electrochemical impedance spectroscopy for lithium-ion cells: Test equipment and procedures for aging and fast characterization in time and frequency domain,” Journal of Power Sources, vol. 273, pp. 613–623, 2015.

[17] D. Klotz, “Characterization and modeling of electrochemical energy conversion systems by impedance techniques,” Ph.D. dissertation, Universität Karlsruhe, 2012.

[18] N. Hallemans, W. D. Widanage, X. Zhu, S. Moharana, M. Rashid, A. Hubin, and J. Lataire, “Operando electrochemical impedance spectroscopy and its application to commercial li-ion batteries,” Journal of Power Sources, vol. 547, p. 232005, 2022.

[19] M. Kuipers, P. Schröer, T. Nemeth, H. Zappen, A. Blömeke, and D. U. Sauer, “An algorithm for an online electrochemical impedance spectroscopy and battery parameter estimation: Development, verification and validation,” Journal of Energy Storage, vol. 30, p. 101517, 2020.

[20] S. R. Islam and S.-Y. Park, “Precise online electrochemical impedance spectroscopy strategies for Li-ion batteries,” IEEE Transactions on Industry Applications, vol. 56, no. 2, pp. 1661–1669, 2019.

[21] M. Messing, T. Shoa, and S. Habibi, “Estimating battery state of health using electrochemical impedance spectroscopy and the relaxation effect,” Journal of Energy Storage, vol. 43, p. 103210, 2021.

[22] S. Tairov and L. Stevanatto, “State-of-charge estimation of lead-acid batteries by using multi-frequency ac tests,” International Journal of Advanced Research in Electrical, Electronics and Instrumentation Engineering, vol. 5, pp. 7984–7991, 2016.

[23] A. De Angelis, E. Buchicchio, F. Santoni, A. Moschitta, and P. Carbone, “Uncertainty characterization of a practical system for broadband measurement of battery eis,” IEEE Transactions on Instrumentation and Measurement, vol. 71, pp. 1–9, 2022.

[24] Y. Fu, J. Xu, M. Shi, and X. Mei, “A fast impedance calculation based battery state-of-health estimation method,” IEEE Transactions onIndustrial Electronics, 2021.

[25] B. Bullecks, R. Suresh, and R. Rengaswamy, “Rapid impedance measurement using chirp signals for electrochemical system analysis,” Computers & Chemical Engineering, vol. 106, pp. 421–436, 2017.

[26] D. Klotz, M. Sch¨onleber, J. Schmidt, and E. Ivers-Tiff´ee, “New approach for the calculation of impedance spectra out of time domain data,” Electrochimica Acta, vol. 56, no. 24, pp. 8763–8769, 2011.

[27] A. Nikolian, J. Jaguemont, J. De Hoog, S. Goutam, N. Omar, P. Van Den Bossche, and J. Van Mierlo, “Complete cell-level lithium-ion electrical ecm model for different chemistries (nmc, lfp, lto) and temperatures (-5° c to 45°c)–optimized modelling techniques,” International Journal of Electrical Power & Energy Systems, vol. 98, pp. 133–146, 2018.

[28] S. S. Madani, E. Schaltz, and S. Knudsen Kær, “An electrical equivalent circuit model of a lithium titanate oxide battery,” Batteries, vol. 5, no. 1, p. 31, 2019.

[29] X.-Z. R. Yuan, C. Song, H. Wang, and J. Zhang, Electrochemical impedance spectroscopy in PEM fuel cells: fundamentals and applications. Springer Science & Business Media, 2009.